Fuel 427 (2027) 139880

Contents lists available at ScienceDirect

Fuel

journal homepage: www.elsevier.com/locate/fuel

Full Length Article

Thermocatalytic transcarbonation with diethyl carbonate for valorization of glycerol – recycling siliceous bauxite residue waste components and exploring the potential of sodalite hydroxide reservoir

Yvette Szabó [a,b], Bence Kutus [a,b], Rebeka Mészáros [c], Péter Bélteky [d], Zoltán Kónya [d,e], Ákos Kukovecz [d], Pál Sipos [a,b], Márton Szabados [a,b,*]

[a] Department of Molecular and Analytical Chemistry, University of Szeged, Dóm tér 8, Szeged H-6720 Hungary
[b] Material and Solution Structure Research Group, Institute of Chemistry, University of Szeged, Aradi vértanúk tere 1, Szeged H-6720 Hungary
[c] Institue of Pharmaceutical Chemistry, University of Szeged, Eötvös utca 6, Szeged H-6720 Hungary
[d] Department of Applied and Environmental Chemistry, University of Szeged, Rerrich B. tér 1, Szeged H-6720 Hungary
[e] HUN-REN-SZTE Reaction Kinetics and Surface Chemistry Research Group, Rerrich B. tér 1, Szeged H-6720 Hungary

ARTICLE INFO

Keywords:
Bauxite residues
Katoites
Sodalites
Earth-abundant catalysts
Glycerol carbonate production
Catalytic dominance of hydroxide cage anions

ABSTRACT

Bauxite residues contain katoites and desilication products (sodalite and cancrinite), which are excellent candidates for Earth-abundant heterogeneous base catalysts from industrial waste sources. For the first time, they were tested in synthetizing the renewable and promising fuel or fuel additive glycerol carbonate for the purpose of recycling glycerol by-products from biodiesel production. Incorporation of silicate was found to enhance the previously established excellent catalytic activity of tricalcium aluminate (Si-free katoite). Performance of sodalites containing four different cage anion-designed (OH, CO_3, SO_4, Cl) and carbonated cancrinite was determined to a much greater extent by their Brönsted OH content than by the basicity of the caged anions. Direct catalytic use of bauxite residue resulted in a glycerol carbonate yield of over 80%, but it was quickly deactivated due to the limited reusability of many of its most active components (*i.e.,* Si-free and Si-containing katoites, chloride sodalites). However, hydroxysodalites showed excellent reusability, with a glycerol carbonate yield of around 80% even after 5 reuses. The activity of katoites and sodalities overtook that of many complex systems containing relatively rare metals, such as Ni, Cu, Zr, and Ce. Their excellent activity has made it possible to use diethyl carbonate solvent/reagent, which is more favourable in terms of sustainability, instead of the more widely applied dimethyl carbonate, even with as short reaction times as 30–60 min.

1. Introduction

Biodiesel production is generally based on the transesterification of vegetable oils and animal fats. This industry went through a remarkable development over the last few years. In addition to the main product, *i.e.,* fatty acid methyl ester, glycerol is produced in a strikingly large amount. This chemical waste is a reactive platform compound, which can be transformed into various other valuable products [1,2]. Glycerol-1,2-carbonate (4-hydroxymethyl-1,3-dioxolan-2-one, GLC) is one of the most valuable and extensively studied chemicals obtained from the transesterification reaction of glycerol, due to its application potential in several fields, such as co-solvent in ionic liquids [3], multipurpose green solvent [4], adhesive, surfactant and lubricant in the cosmetic industry [5,6], electrolyte in Li-ion batteries [7,8] and also as monomer in polymer synthesis [9,10]. Furthermore, carbonate esters can significantly reduce emissions of soot, unburned hydrocarbons, and carbon monoxide. Thus, a few years ago, it has been demonstrated that bio-based GLC has outstanding potential as a sustainable fuel or fuel additive for internal combustion engines due to its high oxygen content and excellent thermal stability (high flash point) [11]. Utility of GLC in the biorefinery economy, whether used directly or as a versatile chemical intermediate, is further aided and enhanced by its numerous beneficial and environmentally friendly properties, such as good biodegradability, water solubility (high moisture retention capacity), low volatility and toxicity, and excellent stability over an extensive temperature range (melting point: −69 °C and boiling point: 354 °C).

* Corresponding author at: Department of Molecular and Analytical Chemistry, University of Szeged, Dóm tér 8, Szeged H-6720 Hungary.
E-mail address: szabados.marton@chem.u-szeged.hu (M. Szabados).

https://doi.org/10.1016/j.fuel.2026.139880
Received 15 March 2026; Received in revised form 30 April 2026; Accepted 9 May 2026
Available online 13 May 2026

The most common industrial GLC production method is based on the reaction of glycerol and phosgene in the presence of alkaline catalysts [12]. Due to the highly toxic and corrosive nature of phosgene, several alternative methods have been developed in recent years. However, these also have some drawbacks, for example: transesterification of glycerol with urea produces large amounts of ammonia as a by-product, which limits their industrial application [13]. Despite the numerous publications in this field [14–17], even the process of atmospheric CO_2 sequestration and direct reaction with glycerol, which is highly advantageous and sustainable in many respects, has not yet been able to deliver the expected results (generally low GLC yields and harsh reaction conditions). As a solution, a technique with relatively few trade-offs could be the transcarbonation of glycerol with organic carbonates, for example using the increasingly studied dimethyl and diethyl carbonate (biodegradability, low toxicity), which are green solvents/reagents in the presence of basic catalysts [5,12,18–23]. They require mild conditions; relatively low temperatures at atmospheric pressure and readily available catalysts of various types, for instances zeolites [1], pure and doped metal oxides [24], calcined or pristine layered double hydroxides [25–27] and even cement or red mud wastes [1,6,28,29].

Hydrogarnets represent a prominent family in the group of garnets, which are minerals containing *ortho*-silicates with a wide selection of compositions and structures. Katoites belong to this family with the $Ca_3Al_2(SiO_4)_{3-x}(OH)_{4x}$ general formula, where $x \geq 1.5$ (often referred to as hydrogrossular, hydrogarnet or hibschite mineral) [30]. In the case where the value of x reaches three, all the silicate groups are replaced by hydroxides and the tricalcium aluminate hexahydrate (TCA, Si-free katoite or C_3AH_6 according to the cement notation) product is obtained [31]. In these crystal structures, which are remarkable from a structural and thus potentially catalytic point of view, Ca atoms have distorted square antiprismatic, Al atoms have octahedral, while Si atoms have tetrahedral geometry. From an industrial aspect, katoites, as reactive phases, are often investigated because of their notably presence in Bauxite Residue (BxR, obtained from red mud by drying and thickening to minimize the amount of strongly alkaline liquid) [32]. Furthermore, they can influence the pumping and the stability of concrete in cementitious systems with different molar ratios of Si/OH replacement [33].

The other catalytically interesting Si-containing basic components of BxR are the hydrated sodium aluminosilicates (feldspathoids), the so-called desilication products (DSPs). Large amount of DSP is formed during the Bayer process, when reactive silica is digested and precipitates capturing significant amounts of sodium ions [34,35]. Various anions (stemming from Bayer liquor) and water molecules are usually present in intraframework cages, such as: chlorides ($Na_8Al_6Si_6O_{24}X$, $X=Cl_2$), hydroxides ($X=(OH)_2$), sulphates ($X=SO_4$) and carbonates ($X=CO_3$). Thus DSPs can be described as a mixture of different anion-containing sodalites (hydrophilic zeolites). Their precipitation in pipelines is a source of a range of technological problems, therefore mechanism and kinetics of the (trans)formation of DSPs are still the subject of research [36,37]. It is important to note that in heat exchangers, sodalites can largely transform into another feldspathoid with similar structure and same composition, known as cancrinite, meaning that these substances are also common components of DSP [38].

In our previous work, the major Si-free components of BxR were systematically investigated as transesterification catalysts in GLC synthesis from various dialkyl carbonates and glycerol. The research highlighted the great potential of the TCA as an Earth-abundant and biocompatible catalyst (since the Si, Al and Ca are the 2nd, the 3rd and 5th most abundant rock-forming elements in the Earth's crust), with a performance to compete with many moderately rare and/or expensive (*e.g.,* Mn, Ni, Cu, Y, Zr and Nb) transition metal-based composites [39].

Although katoites and DSP/sodalites have a relatively extensive literature, to the best of our knowledge, they have never been used directly as base catalysts in transesterifications, whereas the catalytic utilization of red mud and BxR have long been an active area of research. However, the results of these studies can only be interpreted to a limited extent without knowing the catalytic contributions of the individual base components. To address this shortcoming, and as a continuation of our previous work, the goal was to test the main silica-containing BxR components (katoite up to 10 and DSP up to 40 wt% may occur [40]) as catalysts in transcarbonation of glycerol into glycerol carbonate. By exploring their catalytic performance (activity, robustness, reusability), our ultimate aim was detailed understanding of the catalytic potential of bauxite residues in the valorization of glycerol.

2. Experimental

2.1. Materials

Details are given in the Electronic Supporting Information (ESI) document.

2.2. Preparation of TCA and katoites

TCA was synthesized from the starting reagent $Ca_3Al_2O_6$ by the commonly used hydration method, the synthesis conditions being exactly the same as described in our previous work [39]. Katoites were prepared following the literature with slight modifications [41,42]. Under N_2 atmosphere, waterglass and TCA were mixed in water at a solid-to-liquid mass ratio of 1:5, while the amount of Si was varied in wide range. Target compositions of samples were the followings: $Ca_3Al_2(SiO_4)_{0.1}(OH)_{11.6}$ noted as KAT0.1Si, $Ca_3Al_2(SiO_4)_{0.2}(OH)_{11.2}$ (KAT0.2Si), $Ca_3Al_2(SiO_4)_{0.4}(OH)_{10.4}$ (KAT0.4Si), $Ca_3Al_2(SiO_4)_{0.8}(OH)_{8.8}$ (KAT0.8Si). Dispersions were tightly sealed and stirred at room temperature for one week. Finally, solid products were filtered, washed (distilled water), dried (60 °C, overnight) and stored under N_2.

2.3. Synthesis of DSPs, pure sodalites and cancrinites

DSPs were prepared using supersaturated sodium aluminate solution ($[NaOH]_T$ = 4.50 M, $[Al(III)]_T$ = 1.90 M, $[Na_2SO_4]_T$ = 0.05 M, $[Na_2CO_3]_T$ = 0.20 M), mimicking spent liquors typical of the Bayer process (95 °C and 6 h reaction time). As Si source, five commercially available or high-grade natural kaolinite solids (23 g/L) were applied (Eckalite from Imerys Minerals, Alfa Aesar with batch number P01E055, Georgia KGa–1B, Zettlitz/Sedlec and Sigma Aldrich, batch number BCBV6863). Exact chemical composition of DSPs and the description of their syntheses are detailed in our previous paper [37].

Pure sodalites, which are designed to contain only one type of anion in their β-cages, were prepared in a way similar to that of DSPs, with some modifications as described in the literature. For hydroxide-containing sodalite (hydroxysodalite, denoted as OH-SOD), 9 g Eckalite kaolinite was dissolved and stirred in 100 cm^3 concentrated alkaline solution ($[NaOH]_T \approx 19$ M) for 48 h at 95 °C [43]. For chloride (Cl-SOD) [44], carbonate (CO_3-SOD) [45] and sulphate (SO_4-SOD) [46] caged anions, 5.5 g NaCl, 10 g Na_2CO_3 and 13.4 g Na_2SO_4, respectively, was added to 100 cm^3 spent Bayer liquor ($[NaOH]_T = 4.50$ M, $[Al(III)]_T = 1.90$ M) with 5 g of Eckalite. The amount of each anion was significantly excessive in terms of the values required for the charge neutrality of DSP structures. Mixtures were stirred for 24 h at 95 °C. Carbonate-containing cancrinites (CO_3-CAN) were prepared as follows: 5 g of Eckalite and 0.7 g of Na_2CO_3 (to avoid the formation of CO_3-SOD, the amount of carbonates was only minimally excessive) were mixed with 50 cm^3 of NaOH (8 M) solution in an autoclave for 4 days at 230 °C. Filtration, washing, drying and storage steps were the same as for katoites.

2.4. Catalytic transcarbonation of glycerol with diethyl carbonate

Reaction parameters were determined/optimized in our previous experiments using CaIn-LDHs (layered double hydroxides) or TCA as

base catalysts [27,39]. Diethyl carbonate (DEC, 2.9 cm^3), double distilled glycerol (7.05 mmol, diethyl carbonate:glycerol molar ratio of 3.5:1), solid catalysts (45 mg) were mixed in a glass reactor. Under air and reflux conditions (between 126 and ~ 110 °C, as ethanol gradually formed, which has a significantly lower boiling point than the DEC solvent/reagent), the transcarbonation were executed with mechanical stirring (1500 rpm, in preheated oil bath) and 1 h reaction time. At the end of the tests, mixtures were diluted with methanol (to dissolve the unreacted glycerol), and purified on 0.45 μm filters. Catalysts were centrifuged and washed with isopropyl alcohol, dried and stored under N_2. Clear liquid products were analyzed by GC–MS technique (Thermo Scientific Trace 1310 gas chromatograph, ISQ QD single quadrupole mass spectrometer) and ^1H- and ^{13}C NMR (nuclear magnetic resonance) spectroscopy (Bruker Avance NEO 500 spectrometer, 500 MHz) were also used to study by-product formation. Details can be found in our previous work [39].

2.5. Apparatus of structural characterization

Pristine and spent/used catalysts were probed by transmission and attenuated total reflectance (ATR) Fourier-transform infrared (FT-IR) spectroscopies and Raman microscopy, transmission (TEM) and scanning electron microscope coupled with energy dispersive X-ray spectroscopy (SEM-EDX), powder X-ray diffractometry (XRD) using International Centre for Diffraction Data (ICDD) files, N_2 adsorption–desorption analyser with Brunauer-Emmett-Teller (BET) and density functional theory (DFT) methods, inductively coupled plasma mass spectrometry (ICP-MS), total carbon (TC) and thermogravimetric analyses applying mass spectrometer for evolved gas monitoring (TG-MS). Exact experimental conditions are described in the ESI.

3. Results and discussion

3.1. Catalytic performance of katoites

In our previous work, use of the Si-free TCA catalyst resulted in glycerol conversion rates of > 80% and glycerol carbonate yields of > 60% in only 1 h of reaction time [39]. In order to properly assess the potential negative and positive effects of silicate incorporation, we used the same reaction parameters for testing the katoites (Fig. 1A). The increasing Si content resulted in slowly rising glycerol conversion, higher glycerol carbonate yields and roughly constant degree of glycidol formation (valuable for pharmaceutical and polymer industries [47,48], generated from GLC by CO_2 release). In addition, the difference between the maximum yield estimated from the conversions and the sum of glycidol and GLC yields was significantly reduced, thus the incorporation of silicate inhibited the formation of the frequently occurring by-products from glycerol polymerization, GLC condensation and Ca-glycerol formation (from the relatively intense acid-base reaction with catalysts) [27,49]. Based on these results, it can be concluded that incorporating silicates in TCA (which is very common in BxRs) can be considered favorable for glycerol valorizaton; by promoting glycerol transcarbonation, the GLC yield significantly increased, while glycidol formation did not change.

Improvement of the catalytic activity with increasing Si content can be well explained by the gradually increasing specific surface area and total pore volume of the catalysts (Table 1). Initial TCA surface area (~2 m^2/g) can be more than ten times greater with the highest silicate incorporation ratio (21 m^2/g). Meanwhile, pore size distributions gradually changed from the initial most common 5 and 30 nm to the KAT0.8Si sample with predominant 12 and 17 nm pores. N_2 adsorption–desorption analyses showed type III isotherm for the TCA solid, but the isotherms slowly transformed to type IV with slight H3 type hysteresis as a result of growing Si incorporation (Fig. S1 in ESI). This can be linked to the increased appearance of relatively uniform, wedge-shaped pores ranging in size from 10 to 20 nm due to the non-perfect fit of katoite aggregates. It is likely that these spaces were more easily accessible for the catalysis than the 5 nm pores resulting from the porosity of the individual particles.

It is important to note that determining the exact degree of incorporated silicate is quite complicated, due to the relatively mild structural modification caused by low Si content. XRD patterns of TCA (ICCD file number 24–0217) and katoites ($Ca_3Al_2(SiO_4)(OH)_8$#38–0368, $Ca_{2.93}Al_{1.97}Si_{0.64}O_{2.56}(OH)_{9.44}$#84–0917) were absolutely fully superimposable with the only observed difference being the average size of crystallites calculated from the most intense reflections (Fig. S2, Table 1). Silicate incorporation resulted in a significant size reduction

Table 1
Various physicochemical properties of the TCA and katoite catalysts.

Samples	Specific surface area (m^2/g)[a]	Total pore volume (cm^3/g)[b]	Predominant pore diameters (nm)[b]	Average crystallite sizes (nm)[c]	Detected Si:Al molar ratio[d]
TCA	1.9	0.0073	5 and 30	55 and 60	0:2
KAT0.1Si	8.9	0.0421	16 and 30	33 and 35	0.14:2
KAT0.2Si	12.6	0.0775	17 and 30	36 and 35	0.21:2
KAT0.4Si	18.6	0.0786	10, 17 and 30	37 and 36	0.44:2
KAT0.8Si	21.0	0.0978	12, 17 and 30	37 and 37	0.83:2

[a] Calculated from BET absorption isotherms.
[b] Obtained by applying DFT method for the absorption branches.
[c] Estimated on the basis of the Scherrer equation for the two most intense reflections.
[d] Obtained from ICP-MS and SEM-EDX analyses.

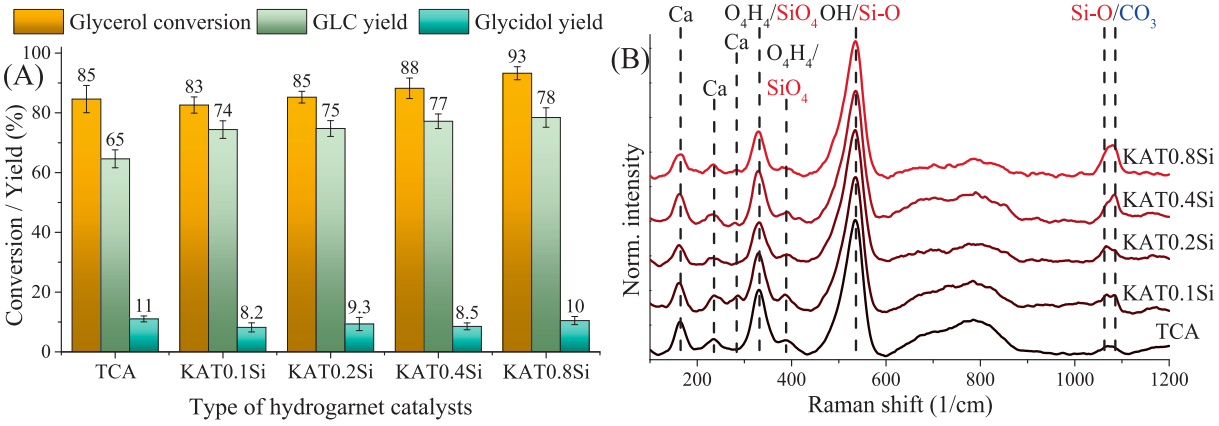

Fig. 1. Testing the catalytic performance of TCA and katoites with growing Si content under reflux for 60 min (A, reaction conditions: 45 mg catalyst, 650 mg glycerol and 3.5:1 DEC:glycerol molar ratio). Raman spectra of the prepared TCA and katoite solids (B).

from ~ 60 to ~ 32 nm, while the increasing Si content caused minimal crystallite growth. There were no reflections connected to by-product formation, only weak baseline elevation could be observed from 15° to 40° 2 theta. Elemental analyses confirmed the target composition of the samples (Table 1). SEM images showed slightly distorted morphology, similar to rhombic dodecahedron, characteristic to both TCA and katoites (Fig. S3) [50–52].

Monitoring silicate incorporation using Raman spectroscopy is limited, as the vibrations of O_4H_4 and SiO_4 tetrahedra are generally difficult to be distinguished [53,54]. As such, Raman analyses of the TCA and katoites did not reveal any significant changes in the spectra with increasing Si content, except for the intensifying vibrations around 1065 and 1085 1/cm (Fig. 1B). These peaks could be associated with the stretching vibrations SiO_4 and surface carbonate groups, respectively [55–57], and are presumably related to the increasing amount of waterglass during synthesis of catalysts. Based on this, it is conceivable that in samples with higher Si content, amorphous (invisible for XRD studies) sodium silicate-type by-products may have formed in larger quantities, which could be responsible for the increase in specific surface area and total pore volume. This is supported by the fact that in solids with Si content greater than 0.2, the pore size distribution changes suddenly, with the amount of 30 nm pores decreasing greatly compared to pores of other sizes (Fig. S1). However, GLC formation was enhanced even at minimal Si content, thus the incorporation of silicate into TCA (*i.e.*, the partially replacement of strong Brönsted base hydroxides with the also strong Lewis basic SiO_4^{4-} units) was clearly beneficial from the catalytic point of view.

3.2. Catalytic tests of DSPs and pure sodalites/cancrinites

To examine the utilization of BxR waste material in glycerol transformation, we carried out catalytic experiments of DSPs by using the same reaction parameters that were applied for the TCA and katoites. First, we investigated the effect of kaolinite origin on DSP generation. In our previous work [37], five kaolinites were tested with slight differences in composition and physicochemical properties, which significantly influenced the kinetics of DSP formation. Glycerol transcarbonation studies have highlighted the catalytic importance of Si sources in Bayer liquor. The Eckalite and Alfa Aesar DSPs, named after the origin of the kaolinites used, showed the highest glycerol conversions, GLC and glycidol yields, while for the Sigma Aldrich, Zettlitz and Georgia DSPs, a remarkable decline was observed in terms of these values (Fig. 2A). Catalytic results were in good agreement with the chemical composition of kaolinites and DSPs (Table S1, S2 and S4 in the ESI of our previous work [37]). Eckalite and Alfa Aesar kaolinites resulted in DSPs with the highest sodalite content (above 85 wt%), while Zettlitz and Sigma Aldrich kaolinites yielded the lowest ones (~58 and ~ 29 wt%, respectively). Despite the significantly low level of sodalite in these two DSPs, they were still able to catalyse the conversion of glycerol to a moderate extent, which may indicate that, in addition to sodalite, the initial kaolinite (~47 wt%) and the forming muscovite (~12 wt%, $(KAl_2(AlSi_3O_{10})(OH)_2)$) phases have also played some catalytic role. These two phases were also present in relatively large quantities in Zettlitz DSP (~23 and ~ 9 wt%, respectively).

SiO_2 content varied widely among DSPs (between 1.3 and 9.5 wt%), but silica appeared to be completely inert in the transcarbonation of glycerol, as did TiO_2 particles, showing less than 5% GLC generation (Fig. S4). Interestingly, Georgia DSP also had high (~80 wt%) sodalite, low SiO_2 and muscovite content (1.4 and 2.7 wt%), but the amount of TiO_2 was the highest (~4 wt%), while in the other DSPs it remained around 1 wt%. Based on this, it could be assumed that the titanium content of the catalysts had some kind of negative effect on the glycerol conversion. To the best of our knowledge, there is no explanation for this in the literature, hence a more in-depth study of this issue may well be important in the future.

After a reaction time of 60 min, Eckalite DSP resulted in conversion and yield similar to that of katoites. Therefore, we studied the reaction kinetics in more detail (Fig. 2B). Maxima of glycerol conversion and GLC/glycidol production could be achieved in just 30 min of reaction time, whereas in our previous work [39], 60–90 min were required for the same conversion using TCA. This was well reflected in the numerical comparison; the glycerol consumption (0.253 mmol/min) and GLC formation rates (0.137 mmol/min, calculated by linear regression of the TCA curves, up to 20 min reaction time) were significantly lower for the Si-free katoite than for DSP catalyst (that data noted in Fig. 2B). Since there were only moderate differences between the catalytic performance of TCA and katoites, it can be assumed that there was a similarly large contrast in the activity of katoites and DSP using only 30 min reaction time. Effect of the stirring rate was also studied, as the high viscosity and relatively low solubility of glycerol in DEC can cause mass transfer limitations, especially at short reaction times [58]. Results were similar to those observed for the TCA catalyst [39], with no significant effect of mixing rate; only when the speed was greatly reduced (from 1500 to 50 rpm), a noticeable decrease was in GLC and glycidol yields (from 74 to 58% and from 17 to 10%, respectively). Conversion of glycerol remained unchanged (92%), indicating an increased degree of side reactions (condensation, polymerization, formation of organic metal salts).

On the basis of the composition of synthesis liquor [37], the cages of DSP sodalities mainly contain hydroxide and also significant amount of carbonate and sulfate anions. In order to examine the catalytic potential

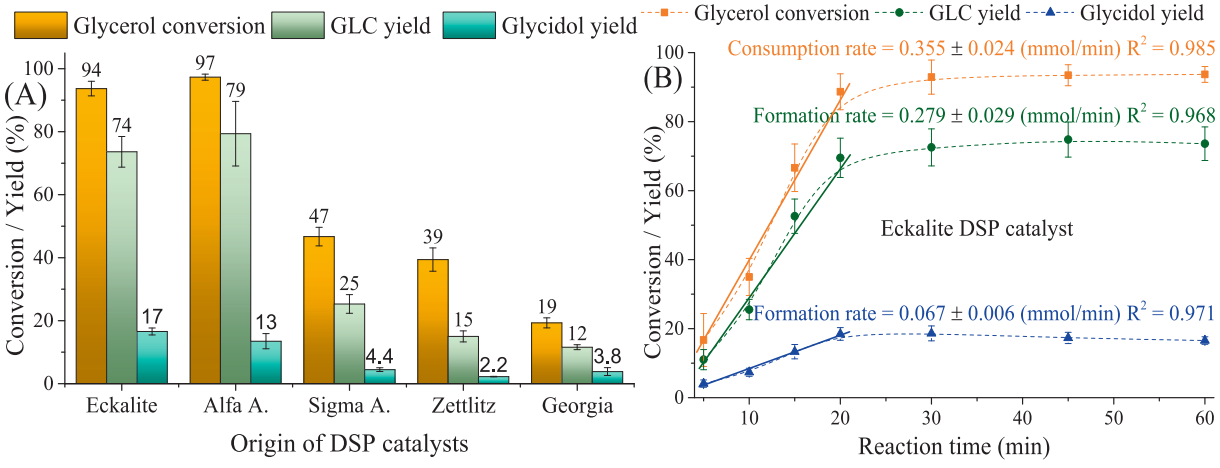

Fig. 2. Study the effect of origin of DSP at 60 min reaction time (A) and the influence of reaction duration using Eckalite DSP (B), reaction conditions: 45 mg catalyst, 650 mg glycerol and 3.5:1 DEC:glycerol molar ratio, reflux.

of pristine solids, we produced and tested sodalites containing only one type of designed anion. We supplemented our investigations with the preparation and catalytic testing of chloride-containing sodalite, as it is often formed during alumina production due to the significant chloride content of bauxite. We also applied carbonated cancrinite, which is readily formed from various sodalites in plants with high operating temperatures. Glycerol conversions showed largely variable catalytic potentials; the most efficient GLC production was obtained using OH-SOD, similar to that observed for Eckalite or Alfa Aesar DSP, while the lowest yields were recorded for SO_4-SOD (Fig. 3A). CO_3-SOD/CAN exhibited similar activity, whereas the performance of the chloride containing SOD was only about 20% lower than the OH-SOD results. No significant difference was observed in the formation of glycidol or by-products between neat sodalite and DSP mixtures, although slightly lower glycidol formation was observed in the case of OH– and Cl-SOD.

Based on XRD measurements, sodalites were produced in a phase pure state, with no identifiable reflections from by-products (Fig. S5). Diffractions were assigned according to the ICCD files of the OH-SOD (#81–0705), Cl-SOD (#82–0517) and CO_3-CAN (#72–2076) phases. Transmission technique made it possible to detect the vibrations of cage anions much more efficiently than using the ATR technique, which is commonly applied in our laboratory [37]. Under 1000 1/cm wavenumber, the symmetric and asymmetric absorption bands of Si/Al – O units can be seen in roughly similar positions (Fig. 3B). Between 3700 and 3000 1/cm, the broad peaks were attributed to the vibrations of crystalline (zeolitic, located in cages) water hydroxyl groups in hydrogen bonding network and to their bending vibrations at 1650 and 1630 1/cm. Signals of incorporated OH anions were around 3635, 3600 and 3530 1/cm and the vibrations attributed to the carbonate and sulfate anions were located at 1475, 1410, 1370 and 1155 1/cm, respectively [59–61]. Therefore, based on FT-IR measurements, the synthesis of the catalysts was also successful, although there were some signs of the incorporation of additional anions, usually hydroxide and carbonate, in addition to the desired anions. Since the cages of SOD and CAN are not permeable to organic substrates as those of zeolites (~0.23 nm vs. ~ 0.74 nm pore windows [62]), catalytic contribution of different types of anions was not expected. However, the magnitude of glycerol transformation differences was surprising, hence we subjected the samples to detailed characterizations.

Starting with N_2 adsorption–desorption analysis (Table 2), the results were quite surprising; the specific surface area and total pore volume of the most catalytically active OH-SOD particles were remarkably lower than those of the other sodalites. The CO_3–, SO_4-, and Cl-SOD values were similar, while CO_3-CAN had a surface area that was only a few m^2/g larger than that of hydroxysodalite. Isotherms were similar; all were type III with slightly varying degrees of H3 hysteresis loops. In terms of pore size distribution, pores around 6 nm dominated in the OH-SOD and CO_3-CAN samples, while larger pores of around 12–16 nm were prevalent in the other solids (Fig. S6, Table 2). The average crystallite sizes calculated from XRD measurements were also similar, ranging between 20 and 55 nm, indicating that there were no significant differences in the crystallinity (Fig. S5, Table 2). A remarkable baseline emergence and the widest reflections were measured for Cl-SOD, indicating lower degree of crystallinity and less favourable incorporation of chloride anions into the forming amorphous aluminosilicate phase, due to the large size and low charge of chloride. The Na:Si:Al molar ratios for OH–, Cl-SOD and CO_3-CAN were as expected (Table 2), while for the SO_4- and CO_3-SOD, minimally Na-deficient systems formed; the slightly different framework of these samples are well-known [45,63].

Table 2
Different physicochemical parameters of the sodalite and cancrinite catalysts.

Samples	Specific surface area (m^2/g)[a]	Total pore volume (cm^3/g)[b]	Predominant pore diameters (nm)[b]	Average crystallite sizes (nm)[c]	Obtained Na:Si:Al molar ratio[d]
OH-SOD	1.1	0.0033	7 and 30	47 and 50	1.33:1:1
CO_3-SOD	27.2	0.0836	9, 12 and 16	35 and 33	1.14:1:1
SO_4-SOD	33.0	0.1135	7, 12 and 16	31 and 27	1.24:1:1
Cl-SOD	30.6	0.0800	7, 17 and 30	25 and 20	1.34:1:1
CO_3-CAN	6.5	0.0160	5, 6 and 30	45 and 46	1.33:1:1

[a] Obtained from BET absorption isotherms.
[b] Obtained by applying DFT method for the absorption branches.
[c] Estimated on the basis of the Scherrer equation for the two most intense reflections.
[d] Calculated by ICP-MS and SEM-EDX analyses.

Surprisingly, no correlation could be found between the physicochemical properties described above and the catalytic performances; in fact, numerous contradictory observations were made. In terms of the reaction mechanism, the following can generally be assumed: in the most important step, the glycerol molecule was deprotonated by the basic centres. Meanwhile, at the acidic sites, DEC could have been adsorbed and activated through the interaction between the oxygen of the carbonyl group and the metal atom. This reduced the electron density at the carbonyl carbon facilitating the nucleophilic attack by the deprotonated glycerol OH group. Since there was no significant difference in the crystal structure of the samples (and even in the specific surface area of the CO_3–, SO_4- and Cl-SOD), the catalytic contribution of the Lewis acid (metal cation) and Lewis base (oxide) units present in

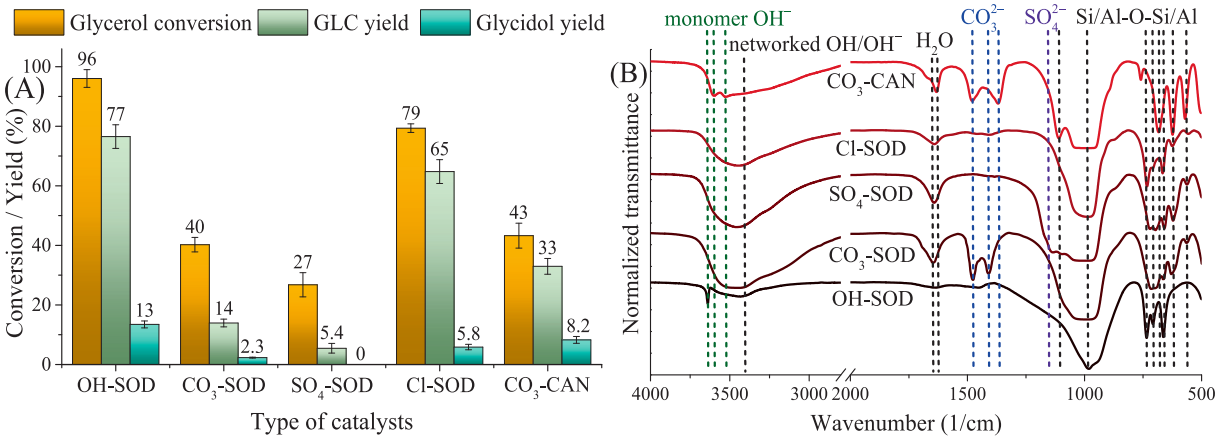

Fig. 3. Probing the catalytic activity of sodalities and cancrinites with various caged anions (A, reaction conditions: 45 mg catalyst, 650 mg glycerol and 3.5:1 DEC: glycerol molar ratio, reflux, 60 min). Transmission infrared spectra of the sodalite and cancrinite samples (B).

them may be similar. This led to the conclusion that cage anions may still play a dominant role in catalytic steps. Since it is highly unlikely that organic molecules can enter and leave the sodalite cages, it must be assumed that inorganic anions, escaped from there and/or interacting while remaining in the cages close to the surface, can activate glycerol molecules through deprotonation. Using this approach, the low activity of the SOD sample containing the least basic sulfate anion can be easily explained, as the more basic carbonate anion filled SOD and CAN solids performed slightly better. Understandably, the highest GLC yield was obtained using OH-SOD containing the strong hydroxide Brönsted base, yet the good performance of the Cl-SOD could not be explained by acid-base effects, even taking into account its considerably higher specific surface area.

It is conceivable that glycerol and its products cooperate strongly with the water content of the catalysts, but these interactions did not appear to affect catalysis, even though there were large differences in the cage water amount (Table 3). For the OH-SODs, in addition to the dominant OH units, weak signals of carbonate anions were also visible. They are likely to originate from small amounts of Na_2CO_3 present in the strongly alkaline Bayer liquor. Band of monomeric OH units could be observed only in the transmission infrared spectrum of this sodalite, the intensity of the vibrations of cage anions and water molecules were compared to the intensity of the peaks of Si/Al − O units in the frameworks under 800 1/cm (Fig. 3B). For CO_3– and SO_4-SOD solids, the amount of desired cage anions was decisive, but they also contained minimal amounts of OH anions (and for SO_4-SOD, some carbonate contamination as well). In contrast, the cages of Cl-SOD contained only about 80 mol% chloride anions, with the remaining 20 mol% being mainly hydroxides and, to a minor extent, carbonate anions. Although chloride anions were used in large excess during the synthesis, OH incorporation was understandably significant, as the amount of Na ($AlOH_4$) in the Bayer liquor was considerable, and the small size of OH anions also facilitated their entry. Based on these findings, it is clear that the Brönsted OH content of sodalite cages was decisive in terms of glycerol conversion.

For CO_3-CAN, carbonate incorporation was incomplete, and a significant amount of OH also entered the cages (Fig. 3B). Thus, activity similar to that of Cl-SOD would be expected, but it is important to note that the specific surface area and total pore volume values of the cancrinite were significantly smaller than that of the Cl-, CO_3– and SO_4-SOD samples. Finally, it can be assumed that the activity of OH-CAN could be similar to that of OH-SOD, which may be worth investigating in more detail in the future. However, due to the very similar thermodynamic stability of CAN and SOD structures, it is quite difficult to produce a pure OH-CAN sample using synthesis parameters similar to those appeared under industrial conditions [64]. It would, therefore, go beyond the scope of this work.

Finally, in an earlier study, we systematically investigated the effects of heat and mechanochemical treatments on the dissolution of kaolinites (through the formation of metakaolinite-type phases) in synthetic Bayer liquor [65]. Even with short grinding times or heat treatments above 500 °C, significant changes were observed in the kinetics of DSP formation, but no remarkable modifications were detected in the composition, crystal structure, and morphology (except for a growth in the size of the lepispheric crystals). Nevertheless, since calcination and grinding of bauxite are common industrial steps, we considered it is important to present their potential effects on the catalytic activity of DSP particles formed. In all cases, pretreatments impaired the performance of DSPs in terms of both conversion and yield (Fig. 4A). Their activity was similar to that of CO_3-SOD and SO_4-SOD, mostly fell between the two.

Transmission infrared spectra showed few but significant differences between the samples, particularly in the intensity of the vibrations of carbonate and sulfate anions relative to each other and to the Si/Al − O units under 800 1/cm (Fig. 4B). Compared to untreated Eckalite DSP, heat treatment and grinding increased the intensity of bands of incorporated sulfate anions (around 1140 1/cm), while those attributed to the caged carbonate anions decreased (at 1475 and 1405 1/cm). Vibrations associated with surface carbonate and kaolinite OH units at 1570 and 3700 1/cm, respectively [37,66], disappeared totally due to the calcination or milling. As a result of the pretreatments, the fraction of SO_4-SOD particles in the DSP increased, and thus their catalytic activity became predominant. This highlighted the fact that, in addition to the composition of the bauxite, the nature of the pretreatments performed prior to its digestion with NaOH is also important, if the anion composition of sodalites extracted from BxR can be of decisive importance for subsequent use.

3.3. *Reusability and comparative studies of BxR and its relevant siliceous components*

Despite the relatively high content of components related to goethite and hematite (~80 wt%, Table S1, proved to be catalytically inactive, Fig. S4) in the BxR tested, particularly good glycerol conversion and GLC production was observed for the first use (Fig. 5A). However, during the second and third uses, there was a significant decline, which may be related to the leaching of soluble alkaline components. This hypothesis was tested by probing the aqueous dispersion (10 mg/cm^3) of the raw and spent (after the first use) BxR solids. After 60 min of stirring at room temperature, the measured pH values (10.8 for raw and 10.3 for spent samples) showed no relevant change in the basicity of solids. Hence, it can be assumed that the variations are clearly related to the deactivation of certain catalytically active phases.

The most active katoite (KAT08.Si, Fig. 5A) exhibited the expected recycling behaviour; previously, the Si-free katoite particles attested similar rapid deactivation without regeneration steps due to the partial dehydration of metal hydroxide units and strong interactions of the Ca (II) ions and glycerol [39]. Interestingly, the reuse potential of sodalites with hydroxide or chloride anions in the cages was found to be remarkably different (Fig. 5B). Hydroxysodalites possessed robust catalytic nature, with glycerol conversion remaining above 90% even after the third use and still around 80% after the sixth use (Fig. S7 for more detailed reuse catalytic data). GLC production increased slightly until the fourth use at the expense of glycidol formation, followed by a slight

Table 3
Water and caged anion content of the sodalite and cancrinite catalysts.

Samples	Presence of cage water[a]	Presence of hydroxyl anions[b]	Presence of carbonate anions[c]	Presence of sulphate anions[d]	Presence of chloride anions[e]
OH-SOD	significant	predominant	minimal	absent	absent
CO_3-SOD	high	minimal	predominant	absent	absent
SO_4-SOD	high	minimal	minimal	predominant	absent
Cl-SOD	standard	significant	minimal	absent	predominant
CO_3-CAN	high	significant	predominant	absent	absent

[a] According to transmission infrared spectra and TG-MS studies, compared to the average composition of $Na_8(Al_6Si_6O_{24})(SO_4)\cdot H_2O$ [62].
[b] According to transmission infrared spectra and TG-MS probes.
[c] According to transmission infrared spectra, TG-MS and TC tests.
[d] According to transmission infrared spectra, TG-MS, ICP-MS and SEM-EDX analyses.
[e] According to TG-MS, ICP-MS and SEM-EDX studies.

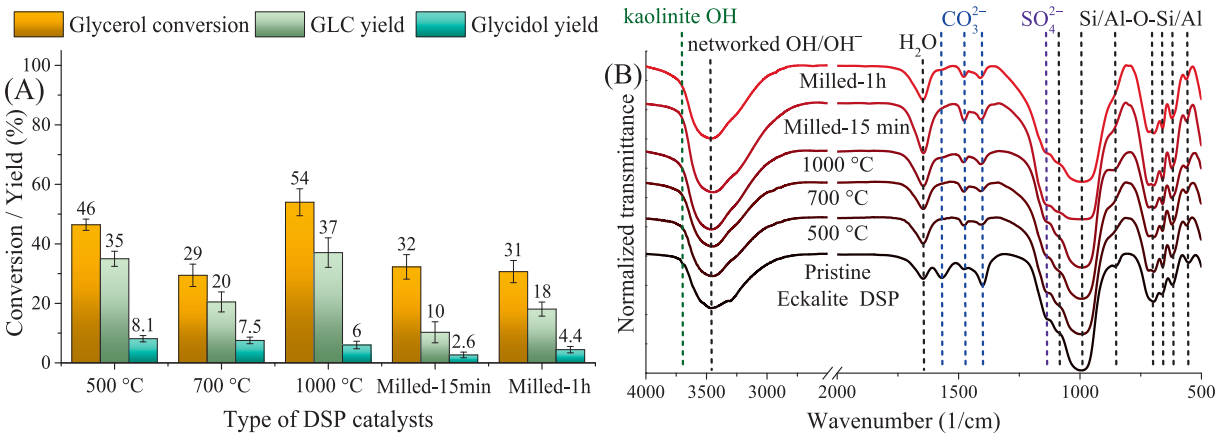

Fig. 4. Investigation of the catalytic potential of various DSP solids prepared from calcined or milled Eckalite kaolinites (A, reaction conditions: 45 mg catalyst, 650 mg glycerol and 3.5:1 DEC:glycerol molar ratio, reflux, 60 min). Transmission infrared spectra of the DSP solids (B).

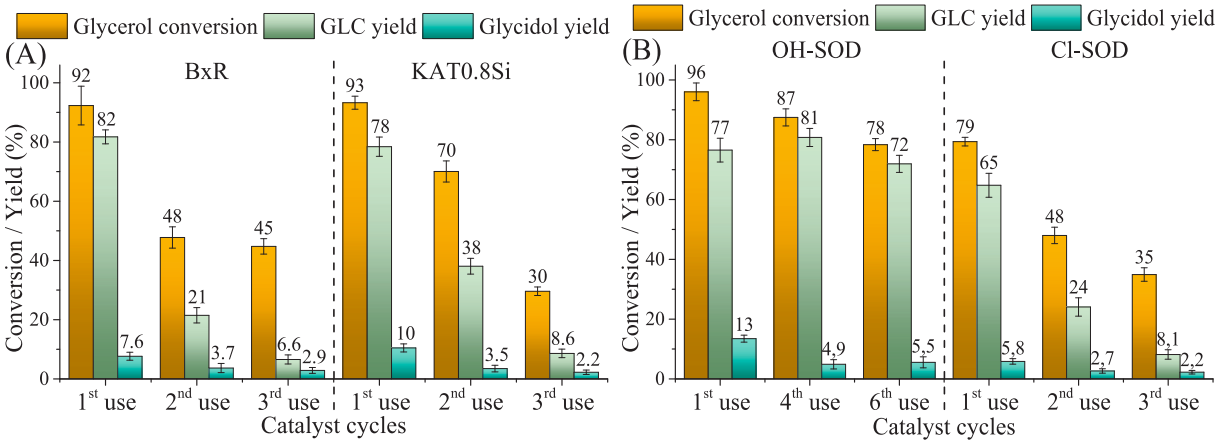

Fig. 5. Catalytic reusability of BxR, katoite (KAT08.Si, containing the highest Si content, A) and hydroxide/chloride containing sodalites (B), reaction conditions: 60 min reaction time, 45 mg catalyst, 650 mg glycerol and 3.5:1 DEC:glycerol molar ratio, reflux.

decrease in GLC yield with stabilized glycidol values. The difference between the sum of GLC and glycidol yields and the glycerol conversion rate also gradually decreased, denoting that by-product formation was suppressed. In contrast, the catalytic performance of Cl-SOD gradually weakened, similarly to TCA and katoite. GLC formation decreased much faster than glycerol conversion, indicating the intense processes of the glycerol-metal salt and/or −polymer generation (no sign of GLC condensed products). These trends explain well the catalytic behaviour upon recycling BxR, since the presence of phases related to katoite (~3.5 wt%) and sodalite (~ 3 wt%, mainly but not solely with hydroxide caged ions) were the most predominant after the iron-containing components. It is important to note that CO_3/OH-CAN was also present in BxR in amounts similar to those of sodalite. Tests showed, however, their role to be probably less significant (Fig. 3B). Similarly, TiO_2 phases (present in ~ 2.5 wt%), and other Ca-based phases ($CaTiO_3$, $CaSiO_3$ in Fig. S4, $Ca(OH)_2$, $CaCO_3$, CaAl/Fe/Ga-LDHs, tested in our previous work [39]), whose total amount was around 2 wt%, did not possess appreciable activity.

More than 200 million tons of red mud are produced annually (based on data from 2025) and it is still almost entirely industrial waste [67]. Therefore, the recycling of BxR is not necessary in its catalytic application for glycerol transcarbonization. However, the chemical composition of the resulting bauxite residues depend on many factors. It is primarily determined by the technology used in alumina production and the chemical quality of the bauxite feedstock (which is strongly influenced by geological conditions). Thus, the quantitative contribution of the components outlined above can certainly show large fluctuations in the catalytic performance. Based on this consideration, we thought it is important to systematically test those BxR components which, due to their quantity and chemical quality, could potentially be active basic catalysts. We have summarized (Table S2) and visualized the results of our previous and current works in Fig. 6. Extracting sodalites from red mud by flotation, centrifugation or selective dissolution, neutralization (which are very complex processes and still require a great deal of development) could mean access to large quantities of valuable catalysts, so it is definitely important to explore the potential for catalytic reuse of these solids.

To understand the difference between the reusability of OH-SOD and Cl-SOD, several characterization techniques were applied for both the unused/pristine and used/spent forms of catalysts. For Cl-SOD, no new reflections were observed and the average size of the crystallites were almost identical before and after the 3rd catalytic use (Fig. S8). The situation was similar in the case of OH-SOD; although the crystallite sizes showed a greater decrease after the sixth use (from 50 to 37 nm), new reflection was not visible, and there was no sign of the non-basic hydrosodalite ($Na_6(Al_6Si_6O_{24})\cdot 4H_2O$ or $8H_2O$, new diffraction peaks between 56° and 69° 2 theta [68]) potentially formed by the leaching of caged anions (Fig. S9). SEM photos clearly showed the lepispheric morphology characteristic to Cl-SOD [69], with an average size of less than 500 nm for both pristine and used solids (Fig. 7 and S10). Particles with different morphologies were not recorded, only a slight deviation was observed after catalysis, the contours of yarn-type lepisheres were

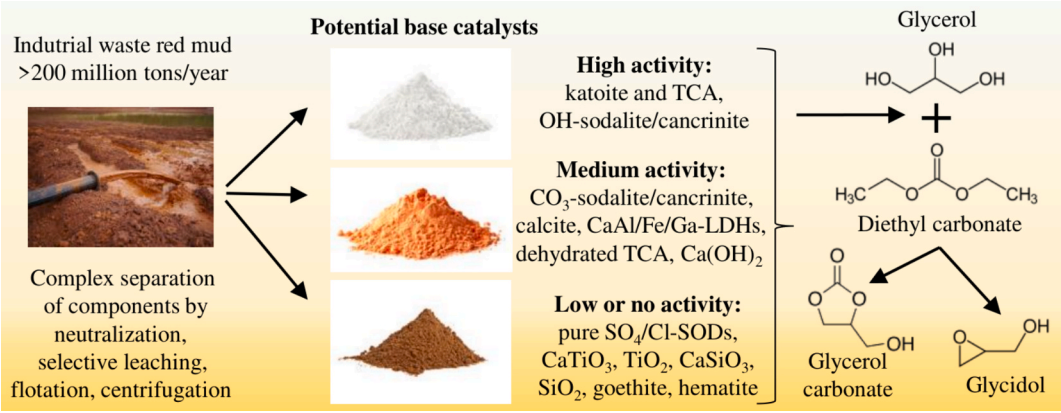

Fig. 6. Infographic summary of catalytic use of BxR components in glycerol transcarbonation.

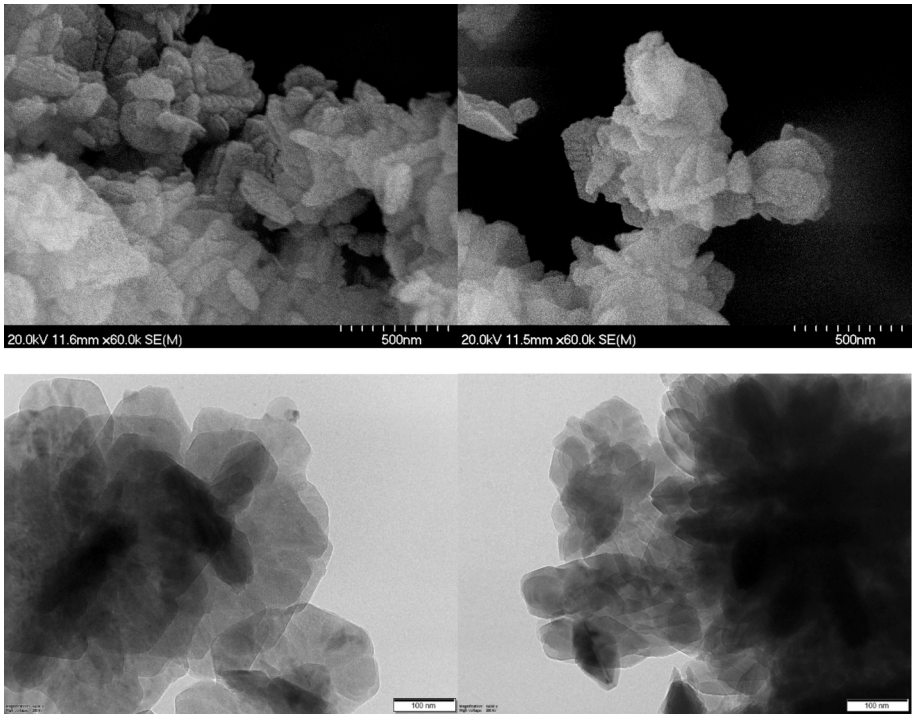

Fig. 7. Electron microscopic photos of the pristine (scanning: top-left, transmission: bottom-left) and spent (after the 3rd cycle, scanning: top-right, transmission: bottom-right) Cl-SODs.

less sharp and distinct. Higher resolution TEM images also confirmed the stable crystal structure of sodalites, but slight aggregation of particles was observed in Cl-SOD as a result of catalysis (Fig. 7 and S11). For OH-SOD, significantly larger particles were observed, with limited possibilities for creating a transparent image, which was to be expected based on the larger crystallite sizes seen in XRD curves. Here, too, it was observed that the extremely sharp contours of particles remained intact even after 6 uses, but there was some visible amorphous surface contamination, presumably organic residue with a higher degree of electron transmission (Fig. S12).

ATR-IR spectra did not reveal organic, physisorbed CO_2 or surface carbonate contaminations for Cl-SOD, and only to a minimal extent in the case of OH-SOD, although these were detected in relevant quantities for katoite (Fig. 8A), just as previously using TCA [39]. Spectra of Cl/OH-SOD showed mainly the characteristic vibrations of the sodalite-type structure: the weak signals of the zeolitic water (around 3300, 1645 1/cm), asymmetric (960, 935 1/cm) and symmetric (~730, ~700 and ~ 660 1/cm) stretching vibrations of the Si/Al – O tetrahedrons [70,71]. Compared to pristine form of sodalites, only the latter bands attested minimal changes during catalysis (Fig. S13). Transmission IR spectra also confirmed the robust structure of sodalites; the water molecules and the minimal amount of carbonate ions in the cages, as well as the structural metal–oxygen vibrations remained virtually unchanged (Fig. S14). For Cl-SOD, after the 3rd use, only weak C – H peaks appeared (~2900 1/cm), while for OH-SOD, after the 6th use, weak C – H (2960, 2925, 2850 1/cm), C=O (1735 1/cm), C – OH (1225 1/cm) and C – C – O (1150 1/cm) vibrations emerged, indicating a slight organic contamination (presumably bands corresponding to glycerol derivatives [39,72]).

Compared to IR measurements, Raman microscopy spectra could provide more surface-specific information; although no signs of organic contaminants were visible this time either, significant changes in crystal structure (not indicated by IR and XRD traces!) were found after catalytic use (Fig. 8B). In the case of OH-SOD, the bending vibrations visible at around 240–260 (Na – O, O – Al – O), 290 1/cm (Al/Si-tetrahedra), 460 1/cm (SiO_4 units), and symmetric and asymmetric stretching

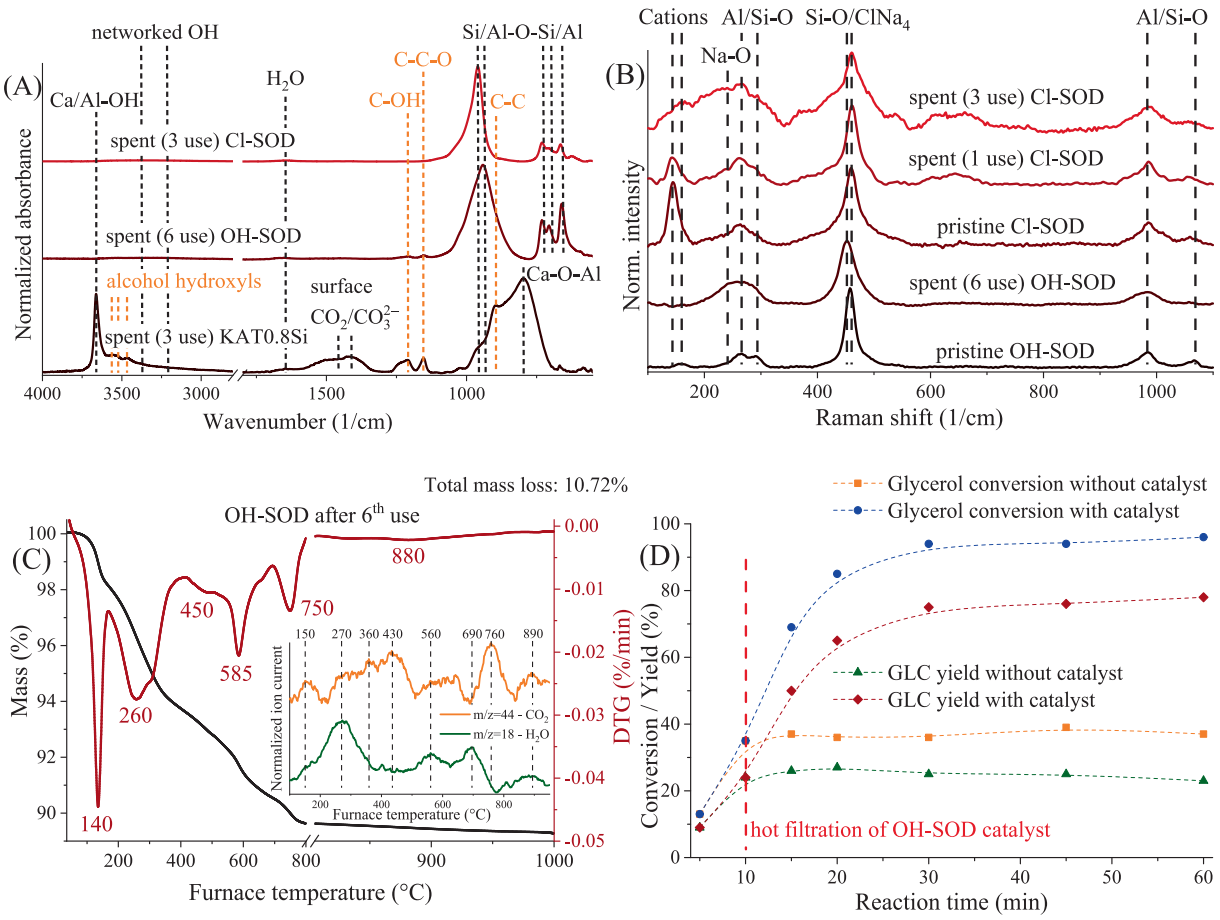

Fig. 8. ATR-IR (A) and Raman (B) spectra of katoite and sodalite samples before and after the catalytic applications. Thermogravimetric, derivative thermogravimetric and evolved gas analysis (C) of spent OH-SOD and hot filtration test (D) of OH-SOD catalyst (reaction conditions: 45 mg catalyst, 650 mg glycerol, 3.5:1 DEC: glycerol molar ratio, reflux).

frequencies at ~ 980 and 1060 ~ 1/cm (Al/Si-tetrahedra, [73]) widened slightly and partially merged, signing the development of irregularity in the chemical environment of the structural elements. For Cl-SOD catalyst, these changes were much more intense (specifically, the weakening of signal 460 1/cm, which could also be related to $ClNa_4$ tetrahedrons, [74]), and the peaks occurring at 145 and 160 1/cm (cationic sublattice vibrations, [75]) completely disappeared during the transcarbonation. Since elemental analysis tests did show only 2–3 at.% loss of Na and Cl ions, it can be assumed that these ions were leached to a greater extent only from the catalytically active external surfaces.

Interestingly, for OH-SOD, nearly 20 at.% of the Na were lost during the 6 uses, but this had only a minimal structural effect on the basic of XRD, IR, and Raman measurements. A comparison of the TG-MS curves of pristine and spent OH-SODs also clearly attested that the sodalite structure underwent only slight modification/damage. Thermal analysis of the initial SOD signed the evaporation of physically adsorbed water molecules until 200 °C, followed by the removal of OH and H_2O content of the cages at around 580, 660, 730, and 860 °C. Decomposition of incorporated carbonate ions contributed to these signals in minimal amount (Fig. S15). These mass losses were also clearly visible during TG-MS analysis of the spent sample, but further peaks were visible at around 260, 450, and 750 °C, accompanied by the departure of CO_2 (Fig. 8C). These were presumably related to the removal of organic pollutants detected by FT-IR test. Based on thermal analysis, even after 6 uses (5 reuses), there was only about 3–4% by weight of organic deposits in the catalysts.

Results of the characterization techniques clearly indicate the highly resistant structure of OH-SOD particles, which explains their more robust catalytic performance compared to Cl-SOD particles. This is accompanied by the rapid depletion of OH content in the cages of Cl-SOD, which resulted in a drastic decrease in glycerol conversion during reuse. As shown by elemental analyses, the OH^- amount (and Na^+, due to charge neutrality) of hydroxysodalite was also significantly reduced, although the starting hydroxide content was much higher. However, it is worth considering the followings: based on the catalytic activity of SO_4-SOD (Fig. 3A), it can be assumed that the Lewis base O_2^- anions in the sodalite structure (and the minimal amount of carbonate caged ions, estimating the sulfate anions to be practically inactive) were only responsible for approximately 25% of the activation of glycerol molecules. Based on these results, during the six uses, ~0.9 mmol OH content (only 20% of which was lost over the course of 6 uses) of the pristine OH-SOD could be responsible for the deprotonation of nearly 28 mmol glycerol, which represents a molar ratio of 1:31. This intense activity clearly shows that OH-SOD could act as a high-capacity and stable solid hydroxide reservoir in the reaction. However, hot filtration tests demonstrated the heterogeneous nature of OH-SOD catalyst (Fig. 8D); glycerol conversion and GLC yield values remained constant after removal of SOD particles by centrifugation. Since the formation enthalpies of basic hydroxysodalite and non-basic hydrosodalite is similar, and the latter is even slightly higher [76], it is difficult to imagine that the OH ions depart and then return to the cages in the bulk phase during catalysis. Based on this, it can be assumed that most of the hydroxide ions participating in and leaving the reaction originated from close to the surface. This explains the heterogeneous catalytic nature and the absence of hydrosodalite formation.

Reuse potential of the KAT0.8Si catalyst will certainly need to be

improved in the future through regeneration steps, as has been done successfully for Si-free catalysts [39], but its initial performance was as excellent as that of OH-SOD. However, it is important to note that the use of highly recyclable hydroxysodalite resulted in a conversion rate of more than 90% even with a reaction time of only 30 min, which was also observed for Eckalite DSP catalyst. Therefore, we thought it would be worthwhile to compare the activity of katoite and sodalite particles with catalysts published in the literature, where various dialkyl carbonates (DAC), namely dimethyl carbonate (DMC) and diethyl carbonate solvents/reagents were used (Table 4). Recently, application of DMC in transcarbonation reactions has become widespread, hence we analyzed our results based on the latest work from the past three-four years. There are still very few examples of the use of DEC, so we took less recent research here. Comparing catalytic performances was greatly complicated by the fact that there was considerable variation in when atmospheric, reflux systems and when high-pressure, closed autoclaves were used. In the latter case, glycidol formation can be significantly reduced (due to CO_2 release), while in the former case, most of the publications reported only an initial reaction temperature. When DAC compounds are utilized as solvents/reagents, the boiling point of the mixture can be significantly reduced due to the alcohol by-products formation. For a more accurate comparison, the heating conditions used are also indicated in the Table 4.

Taking these aspects into account, it can be stated that the use of Si-containing katoite and hydroxysodalite resulted in GLC production levels similar to those reported for CeNi/Cd or (Na/Ca/Mg)/Al oxide-based catalysts with DEC. However, at the same high or just slightly lower temperatures, these catalysts always required significantly longer reaction times (generally 5–10 times higher, Table 4). Choice of DMC meant that lower reaction temperatures were required for GLC syntheses, as we had previously experienced with TCA and testing various DACs. It is likely that the strongly basic OH groups present in the sodalite and katoite systems enhanced the side reactions of glycerol polymerization and organic metal salt formation, resulting in a slightly lower GLC selectivity compared to other catalysts. However, even in this comparison (without considering the differences in reaction temperature), it was clear that the GLC yields achieved with KAT0.8Si and OH-SOD were greater than or comparable to the GLC productions obtained with various catalysts containing alkali, alkaline earth or transition metal oxides. In fact, the reaction times here also significantly exceeded (by a factor 2–5) the times required for our katoite and sodalite catalysts. Only two functionalized carbon-based, relatively complex composite systems (Carbon/SO_3Na, pyrolyzed Na alginate) could achieve comparable GLC yields with similarly short reactions.

Although both DACs can be produced from the direct reaction of alcohols and carbon dioxide (thus contributing to solving the problem of CO_2 emissions) [91], and both compounds have similarly favorable market prices, yet DMC research is much more common, as generally the use of DEC in transesterifications requires higher temperatures, pressures, DEC/glycerol molar ratios, and longer reaction times [92]. However, with the use of a sufficiently active catalyst (based on our work, these could be katoites and sodalites), the advantage of DMC may be lost, and the indisputable benefits of DEC in terms of industry and sustainability can prevail. Such favorable factors include the followings: compared to DMC, the DEC can also be synthetized from biologically produced ethanol, and offers safer transportation/storage and utilization potential due to its higher boiling and flash points. Furthermore, it is known from the literature that, unlike the DMC/glycerol/methanol mixture, the DEC/glycerol/ethanol system does not form an azeotrope [93], which makes the purification, separation, and recirculation of reagents more economical.

4. Conclusions

Continuing our previous work, we mapped the catalytic potential of the major Si-containing components of bauxite residues, that is, katoites and desilication products (mainly sodalities, cancrinites) in sustainable synthesis of glycerol carbonate. Rapid deactivation was observed due to intense surface interactions for katoite, however, the incorporation of *ortho*-silicate units into the tricalcium aluminate structure could be exploited well from a catalytic point of view.

During the examination of the performance of desilication products, it was established that the origin of kaolinite, which dissolves in Bayer liquor as reactive silica, was decisive, and similar observations could be made in relation to the thermal and mechanical pretreatments. By synthesizing and catalytically testing four different caged anion-containing sodalites, the absolute dominance of strongly basic OH ions in catalysis was clearly demonstrated. The surprisingly good catalytic activity of chloride-containing sodalite was due solely to the OH anions incorporated beside the chlorides in larger quantities into the cages.

Bauxite residues, exhibiting excellent catalytic performance, showed rapid deactivation, which can be explained by the limited reusability of the active components. Detailed investigations indicated that, unlike katoite and chloride containing sodalite components, hydroxysodalite was highly reusable up to five times thanks to the robust structure and relatively large hydroxide content. It acted as solid hydroxide reservoir, which counterbalanced the small specific surface area. Therefore, we believe that by increasing the surface area, hydroxysodalite could be an outstanding and unparalleled candidate for catalyst or catalyst support in base-catalyzed reactions.

Finally, our research showed which solid red mud compounds are excellent catalysts for glycerol transcarbonization. These materials are

Table 4
Summary comparing previous heterogeneous catalytic results.

Catalyst	Glycerol conversion (%)	GLC yield (%)	Reaction time (min)	Reaction temperature (°C)	DAC	Ref.
KAT0.8Si	93	78	60	126–110 (rf)	DEC	this work
OH-SOD	94	75	30	126–110 (rf)	DEC	this work
Mg/Al oxide	98	65	600	130 (rf)	DEC	[77]
Ce/Ni oxide	82	82	360	85 (nd)	DEC	[78]
Ce/Cd oxide	91	89	240	100 (nd)	DEC	[79]
Ca/Al oxide	90	83	300	130 (rf)	DEC	[80]
Na/Al oxide	92	91	180	90 (rf)	DEC	[81]
LTA zeolite	78	78	240	90 (ac)	DMC	[1]
Carbon/SO_3Na	73	73	60	90 (nd)	DMC	[82]
Li/Mg composite	92	91	120	80 (rf)	DMC	[83]
Na/La oxide	85	60	120	70 (ac)	DMC	[84]
Zr/Al oxide	98	90	90	110 (ac)	DMC	[85]
Mg/Al/Cu/Zn oxide	96	82	270	85 (rf)	DMC	[86]
Li/MCM41 silica	60	59	165	86 (rf)	DMC	[87]
Mg/Fe oxide	91	86	150	90 (rf)	DMC	[88]
Pyrolyzed Na alginate	93	57	30	75 (rf)	DMC	[89]
Cu/Zn/Mn oxide	99	98	90	90 (rf)	DMC	[90]

ac-autoclave; nd-no data, presumably open system; rf-reflux.

not only industrial wastes, but their metal components are also extremely common on Earth, making them biocompatible and easily accessible for artificial production. Thus, they meet modern sustainability requirements. Thanks to their excellent catalytic performance, it was also possible to validate the use of diethyl carbonate, which is again much more advantageous in terms of sustainability than the more widely used dimethyl carbonate.

CRediT authorship contribution statement

Yvette Szabó: Writing – original draft, Visualization, Validation, Methodology, Investigation, Data curation, Conceptualization. **Bence Kutus:** Writing – review & editing, Validation, Investigation, Formal analysis. **Rebeka Mészáros:** Methodology, Investigation, Data curation. **Péter Bélteky:** Methodology, Investigation, Data curation. **Zoltán Kónya:** Resources. **Ákos Kukovecz:** Resources. **Pál Sipos:** Writing – review & editing, Validation, Resources, Funding acquisition. **Márton Szabados:** Writing – review & editing, Visualization, Validation, Supervision, Project administration, Methodology, Investigation, Funding acquisition, Formal analysis, Data curation, Conceptualization.

Declaration of competing interest

The authors declare the following financial interests/personal relationships which may be considered as potential competing interests: Bence Kutus reports financial support was provided by Hungarian Academy of Sciences (MTA). Marton Szabados reports financial support was provided by Hungarian Academy of Sciences (MTA). Marton Szabados reports financial support was provided by National, Research, Development and Innovation Office. Bence Kutus reports financial support was provided by National Research, Development and Innovation Office. Marton Szabados reports financial support was provided by Emirates Global Aluminum PJSC. If there are other authors, they declare that they have no known competing financial interests or personal relationships that could have appeared to influence the work reported in this paper.

Acknowledgement

Márton Szabados gratefully acknowledges the support of Bolyai Janos Research Fellowship (BO/00246/21/7) of the Hungarian Academy of Sciences (MTA) and the ÚNKP-23-5-SZTE-714 New National Excellence Program of the Ministry for the Innovation and Technology from the Source of the National Research, Development and Innovation Office (NKFIH). Bence Kutus is grateful for financial support of Bolyai Janos Research Fellowship (BO/00551/23/7, MTA) and OTKA Postdoctoral Grant (PD 146529, NKFIH). This work was partly financed by Emirates Global Aluminum PJSC, Abu Dhabi, United Arab Emirates.

Appendix A. Supplementary data

Supplementary data to this article can be found online at https://doi.org/10.1016/j.fuel.2026.139880.

Data availability

Data will be made available on request.

References

[1] Kowalska-Kuś J, Held A, Nowińská K, Góra-Marek K. LTA zeolites as catalysts for transesterification of glycerol with dimethyl carbonate. Fuel 2024;362:130757. https://doi.org/10.1016/j.fuel.2023.130757.
[2] S.L. Barbosa, D.L. Nelson, L. Paconio, M. Pedro, W.T.P. Dos Santos, A.P. Wentz, F.L. Pessoa, F.A. Agblevor, D.A. Bortoleto, M.B. de Freitas-Marques, Environmentally friendly new catalyst using waste alkaline solution from aluminum production for the synthesis of biodiesel in aqueous medium, Bioengineering 10 (2023) 692. https://doi.org/ 10.3390/bioengineering10060692.
[3] Benoit M, Brissonnet Y, Guélou E, De Oliveira Vigier K, Barrault J, Jérôme F. Acid-catalyzed dehydration of fructose and inulin with glycerol or glycerol carbonate as renewably sourced co-solvent. ChemSusChem 3 2010:1304–9. https://doi.org/10.1002/cssc.201000162.
[4] Lameiras P, Boudesocque L, Mouloungui Z, Renault J-H, Wieruszeski J-M, Lippens G, et al. Glycerol and glycerol carbonate as ultraviscous solvents for mixture analysis by NMR. J Magn Reson 2011;212:161–8. https://doi.org/10.1016/j.jmr.2011.06.021.
[5] Simanjuntak FSH, Kim TK, Lee SD, Ahn BS, Kim HS, Lee H. CaO-catalyzed synthesis of glycerol carbonate from glycerol and dimethyl carbonate: Isolation and characterization of an active Ca species. App Catal A-Gen 2011;401:220–5. https://doi.org/10.1016/j.apcata.2011.05.024.
[6] Das B, Mohanty K. A green and facile production of catalysts from waste red mud for the one-pot synthesis of glycerol carbonate from glycerol. J Environ Chem Eng 2019;7:102888. https://doi.org/10.1016/j.jece.2019.102888.
[7] Hu J, Li J, Gu Y, Guan Z, Mo W, Ni Y, et al. Oxidative carbonylation of glycerol to glycerol carbonate catalyzed by $PdCl_2$(phen)/KI. App Catal A-Gen 2010;386:188–93. https://doi.org/10.1016/j.apcata.2010.07.059.
[8] Ochoa-Gómez JR, Gómez-Jiménez-Aberasturi O, Ramirez-Lopez C, Belsué M. A Brief review on industrial alternatives for the manufacturing of glycerol carbonate. Org Process Res Dev 2012;16:389–99. https://doi.org/10.1021/op200369v.
[9] Ubaghs L, Fricke N, Keul H, Höcker H. Polyurethanes with pendant hydroxyl groups: Synthesis and characterization. Macromol Rapid Comm 2004;25:517–21. https://doi.org/10.1002/marc.200300064.
[10] Rokicki G, Rakoczy P, Parzuchowski P, Sobiecki M. Hyperbranched aliphatic polyethers obtained from environmentally benign monomer: glycerol carbonate. Green Chem 2005;7:529–39. https://doi.org/10.1039/B501597A.
[11] Szőri M, Giri BR, Wang Z, Dawood AE, Viskolcz B, Farooq A. Glycerol carbonate as a fuel additive for a sustainable future, sustainable. Energy Fuels 2018;2:2171–8. https://doi.org/10.1039/C8SE00207J.
[12] Sahani S, Upadhyay SN, Sharma YC. Critical review on production of glycerol carbonate from byproduct glycerol through transesterification. Ind Eng Chem Res 2021;60:67–88. https://doi.org/10.1021/acs.iecr.0c05011.
[13] Sonnati MO, Amigoni S, de Givenchy EPT, Darmanin T, Choulet O, Guittard F. Glycerol carbonate as a versatile building block for tomorrow: synthesis, reactivity, properties and applications. Green Chem 2013;15:283–301. https://doi.org/10.1039/C2GC36525A.
[14] Li H, Jiao X, Li L, Zhao N, Xiao F, Wei W, et al. Synthesis of glycerol carbonate by direct carbonylation of glycerol with CO_2 over solid catalysts derived from Zn/Al/La and Zn/Al/La/M (M = Li, Mg and Zr) hydrotalcites, Catal. Sci Technol 2015;5:989–1005. https://doi.org/10.1039/C4CY01237B.
[15] Liu J, Li Y, Zhang J, He D. Glycerol carbonylation with CO_2 to glycerol carbonate over CeO_2 catalyst and the influence of CeO_2 preparation methods and reaction parameters. App Catal A-Gen 2016;513:9–18. https://doi.org/10.1016/j.apcata.2015.12.030.
[16] Su X, Lin W, Cheng H, Zhang C, Wang Y, Yu X, et al. Metal-free catalytic conversion of CO_2 and glycerol to glycerol carbonate. Green Chem 2017;19:1775–81. https://doi.org/10.1039/C7GC00260B.
[17] Procopio D, Di Gioia ML. An overview of the latest advances in the catalytic synthesis of glycerol carbonate. Catalysts 2022;12:50. https://doi.org/10.3390/catal12010050.
[18] Ochoa-Gómez JR, Gómez-Jiménez-Aberasturi O, Maestro-Madurga B, Pesquera-Rodríguez A, Ramírez-López C, Lorenzo-Ibarreta L, et al. Synthesis of glycerol carbonate from glycerol and dimethyl carbonate by transesterification: catalyst screening and reaction optimization. App Catal A-Gen 2009;366:315–24. https://doi.org/10.1016/j.apcata.2009.07.020.
[19] Takagaki A, Iwatani K, Nishimura S, Ebitani K. Synthesis of glycerol carbonate from glycerol and dialkyl carbonates using hydrotalcite as a reusable heterogeneous base catalyst. Green Chem 2010;12:578–81. https://doi.org/10.1039/B925404H.
[20] Kumar A, Iwatani K, Nishimura S, Takagaki A, Ebitani K. Promotion effect of coexistent hydromagnesite in a highly active solid base hydrotalcite catalyst for transesterifications of glycols into cyclic carbonates. Catal Today 2012;185:241–6. https://doi.org/10.1016/j.cattod.2011.08.016.
[21] Simanjuntak FSH, Widyaya VT, Kim CS, Ahn BS, Kim YJ, Lee H. Synthesis of glycerol carbonate from glycerol and dimethyl carbonate using magnesium–lanthanum mixed oxide catalyst. Chem Eng Sci 2013;94:265–70. https://doi.org/10.1016/j.ces.2013.01.070.
[22] Zheng L, Xia S, Lu X, Hou Z. Transesterification of glycerol with dimethyl carbonate over calcined Ca-Al hydrocalumite. Chinese J Catal 2015;36:1759–65. https://doi.org/10.1016/S1872-2067(15)60915-9.
[23] Praikaew W, Kiatkittipong W, Aiouache F, Najdanovic-Visak V, Termtanun M, Lim JW, et al. Mechanism of CaO catalyst deactivation with unconventional monitoring method for glycerol carbonate production via transesterification of glycerol with dimethyl carbonate. Int J Energy Res 2021;46:1646–58. https://doi.org/10.1002/er.7281.
[24] Parameswaram G, Srinivas M, Hari Babu B, Sai Prasad PS, Lingaiah N. Transesterification of glycerol with dimethyl carbonate for the synthesis of glycerol carbonate over Mg/Zr/Sr mixed oxide base catalysts. Cat Sci Technol 2013;3:3242–9. https://doi.org/10.1039/C3CY00532A.
[25] Álvarez MG, Plíšková M, Segarra AM, Medina F, Figueras F. Synthesis of glycerol carbonates by transesterification of glycerol in a continuous system using

supported hydrotalcites as catalysts. App Catal B-Environ 2012;113–114:212–20. https://doi.org/10.1016/j.apcatb.2011.11.040.
[26] Szabados M, Mészáros R, Erdei S, Kónya Z, Kukovecz Á, Sipos P, et al. Ultrasonically-enhanced mechanochemical synthesis of CaAl-layered double hydroxides intercalated by a variety of inorganic anions. Ultrason Sonochem 2016; 31:409–16. https://doi.org/10.1016/j.ultsonch.2016.01.026.
[27] Szabados M, Ádám AA, Traj P, Muráth S, Baán K, Bélteky P, et al. Mechanochemical and wet chemical syntheses of CaIn-layered double hydroxide and its performance in a transesterification reaction compared to those of other Ca2M(III) hydrocalumites (M: Al, Sc, V, Cr, Fe, Ga) and Mg(II)-, Ni(II)-, Co(II)- or Zn(II)-based hydrotalcites. J Catal 2020;391:282–97. https://doi.org/10.1016/j.jcat.2020.07.038.
[28] Kumar D, Singh B, Banerjee A, Chatterjee S. Cement wastes as transesterification catalysts for the production of biodiesel from Karanja oil. J Clean Prod 2018;183: 26–34. https://doi.org/10.1016/j.jclepro.2018.02.122.
[29] Wang B, Li S, Tian S, Feng R, Meng Y. A new solid base catalyst for the transesterification of rapeseed oil to biodiesel with methanol. Fuel 2013;104: 698–703. https://doi.org/10.1016/j.fuel.2012.08.034.
[30] Sacerdoti M, Passaglia E. The crystal structure of katoite and implications within the hydrogrossular group of minerals. Bull Minéral 1985;108:1–8. https://doi.org/10.3406/BULMI.1985.7852.
[31] Geiger CA, Dachs E, Benisek A. Thermodynamic behavior and properties of katoite (hydrogrossular): a calorimetric study. Am Mineral 2012;97:1252–5. https://doi.org/10.2138/am.2012.4106.
[32] Maeda H, Kurosaki Y, Nakamura T, Nakayama M, Ishida EH, Kasuga T. Control of chemical composition of hydrogrossular prepared by hydrothermal reaction. Mater Lett 2014;131:132–4. https://doi.org/10.1016/j.matlet.2014.05.168.
[33] Frías M, Martínez-Ramírez S, de la Villa RV, García-Giménez R, de Rojas MS. New scientific evidence of the effect of high temperatures and long curing times on MK-blended cement paste mineralogy. Cement Concrete Res 2022;152:106657. https://doi.org/10.1016/j.cemconres.2021.106657.
[34] Ho GE, Robertson WA, Roach GI, Antonovsky A. Morphological study of Bayer process desilication product and its application to laboratory and plant digests. Ind Eng Chem Res 1992;31:982–6. https://doi.org/10.1021/ie00003a047.
[35] Sun Y, Pan A, Ma Y, Chang J. Extraction of alumina and silica from high-silica bauxite by sintering with sodium carbonate followed by two-step leaching with water and sulfuric acid. RSC Adv 2023;13:23254–66. https://doi.org/10.1039/D3RA03362G.
[36] Smith P. The processing of high silica bauxites — Review of existing and potential processes. Hydrometall 2009;98:162–76. https://doi.org/10.1016/j.hydromet.2009.04.015.
[37] Kása E, Szabados M, Baán K, Kónya Z, Kukovecz Á, Kutus B, et al. The dissolution kinetics of raw and mechanochemically treated kaolinites in industrial spent liquor – the effect of the physico-chemical properties of the solids. App Clay Sci 2021;203: 105994. https://doi.org/10.1016/j.clay.2021.105994.
[38] Barnes MC, Addai-Mensah J, Gerson AR. A methodology for quantifying sodalite and cancrinite phase mixtures and the kinetics of the sodalite to cancrinite phase transformation. Micropor Mesopor Mater 1999;31:303–19. https://doi.org/10.1016/S1387-1811(99)00080-3.
[39] Szabó Y, Nagy SB, Ádám AA, Mészáros R, Kónya Z, Kukovecz Á, et al. Valorization of glycerol to glycerol carbonate and glycidol by different dialkyl carbonates utilizing tricalcium aluminate hexahydrate as transesterification catalyst. ChemCatChem 2025;17:e202401217. https://doi.org/10.1002/cctc.202401217.
[40] J. Vogrin, H. Hodge, T. Santini, H. Peng, J. Vaughan, Quantitative X-ray diffraction study into bauxite residue mineralogical phases, C. Chesonis (Ed.), Light Metals 2019. The Minerals, Metals & Materials Society, Pittsburgh, PA (2019), pp. 93-99.
[41] Jappy TG, Glasser FP. Quantitative synthesis and stability of silica-substituted hydrogarnet $Ca_3Al_2Si_{3-x}O_{12-4x}(OH)_{4x}$. Adv Chem Res 1991;4:1–8. https://doi.org/10.1680/adcr.1991.4.1.1.
[42] Dilnesa BZ, Lothenbach B, Renaudin G, Wichser A, Kulik D. Synthesis and characterization of hydrogarnet $Ca_3(Al_xFe_{1-x})_2(SiO_4)_y(OH)_{4(3-y)}$. Cem Concr Res 2014;59:96–111. https://doi.org/10.1016/j.cemconres.2014.02.001.
[43] Peng H, Kim T, Vaughan J. Acid leaching of desilication products: Implications for acid neutralization of bauxite residue. Ind Eng Chem Res 2020;59:8174–82. https://doi.org/10.1021/acs.iecr.0c00423.
[44] J. Vogrin, T. Santini, H. Peng, J. Vaughan, Influence of chloride on sodium aluminosilicate solubility in Bayer liquor, Micropor. Mesopor. Mat. 299 (2020) 110086. Doi: 10.1016/j.micromeso.2020.110086.
[45] Hermeler G, Buhl J-C, Hoffmann W. The influence of carbonate on the synthesis of an intermediate phase between sodalite and cancrinite. Catal Today 1991;8: 415–26. https://doi.org/10.1016/0920-5861(91)87020-N.
[46] Vogrin J, Peng H, Santini T, Lee LJ, Vaughan J. The influence of sodium sulphate on sodium aluminosilicate solubility in Bayer liquor aiding the desilication process. Hydrometall 2023;219:106079. https://doi.org/10.1016/j.hydromet.2023.106079.
[47] Prete P, Cespi D, Passarini F, Capacchione C, Proto A, Cucciniello R. Glycidol syntheses and valorizations: boosting the glycerol biorefinery. Curr Opin Green Sustain Chem 2022;35:100624. https://doi.org/10.1016/j.cogsc.2022.100624.
[48] Vandenberg EJ. Polymerization of glycidol and its derivatives: a new rearrangement polymerization. J Polym Sci: Polymer Chemistry Edition 1985;23: 915–49. https://doi.org/10.1002/pol.1985.170230401.
[49] Li J, Wang T. On the deactivation of alkali solid catalysts for the synthesis of glycerol carbonate from glycerol and dimethyl carbonate. Reac Kinet Mech Cat 2011;102:113–26. https://doi.org/10.1007/s11144-010-0259-y.
[50] Whittington BI, Fallows TM, Willing MJ. Tricalcium aluminate hexahydrate TCA filter aid in the Bayer industry: factors affecting TCA preparation and morphology. Int J Miner Process 1997;49:1–29. https://doi.org/10.1016/S0301-7516(96)00035-X.
[51] Kyritsis K, Meller N, Hall C. Chemistry and morphology of hydrogarnets formed in cement-based CASH hydroceramics cured at 200° to 350 °C. J Am Ceram Soc 2009; 92:1105–11. https://doi.org/10.1111/j.1551-2916.2009.02958.x.
[52] Shevchenko A, Morell K, Moudrakovski I, Lotsch B, Dinnebier R, Bette S. Stabilization of the garnet lattice by silicon incorporation in polycrystalline katoite. Dalton Trans 2025;54:12157–68. https://doi.org/10.1039/D5DT01202C.
[53] E. Knittle, A. Hathorne, M. Davis, Q. Williams, A spectroscopic study of the high-pressure behavior of the O_4H_4 substitution in garnet, In High-Pressure Research: Application to Earth and Planetary Sciences; Syono, Y., Manghnani, M. H., Eds.; Terra Scientific Publishing Company (TERRAPUB), Tokyo/American Geophysical Union: Washington D.C., 1992; pp 297−304. Doi: 10.1029/GM067p0297.
[54] Kolesov BA, Geiger CA. The vibrational spectrum of synthetic hydrogrossular (katoite) $Ca_3Al_2(O_4H_4)_3$: a low-temperature IR and Raman spectroscopic study. Am Mineral 2005;90:1335–41. https://doi.org/10.2138/am.2005.1622.
[55] Osipov A, Osipova L, Zainullina R. Raman spectroscopy and statistical analysis of the silicate species and group connectivity in cesium silicate glass forming system. Int J Spectrosc 2015;2015:572840. https://doi.org/10.1155/2015/572840.
[56] Zinkevich T, Fiedler A, Guin M, Tietz F, Guillon O, Ehrenberg H, et al. Na^+ ion mobility in $Na_{3+x}Sc_2(SiO_4)_x(PO_4)_{3-x}$ ($0.1 < x < 0.8$) observed by ^{23}Na NMR spectroscopy. Solid State Ionics 348 2005:115277. https://doi.org/10.1016/j.ssi.2020.115277.
[57] Mohsin H, Maron S, Maurin I, Burov E, Tricot G, Devys L, et al. Thermal behavior of waterglass: foaming and xerogel-to-glass evolution. J Non-Cryst- Solids 2021; 566:120872. https://doi.org/10.1016/j.jnoncrysol.2021.120872.
[58] Esteban J, Ladero M, Molinero L, García-Ochoa F. Liquid–liquid equilibria for the ternary systems DMC–methanol–glycerol, DMC–glycerol carbonate–glycerol and the quaternary system DMC–methanol–glycerol carbonate–glycerol at catalytic reacting temperatures. Chem Eng Res Des 2014;92:2797–805. https://doi.org/10.1016/j.cherd.2014.05.026.
[59] Kloprogge JT, Wharton D, Hickey L, Frost RL. Infrared and Raman study of interlayer anions CO_3^{2-}, NO_3^-, SO_4^{2-} and ClO_4^- in Mg/Al-hydrotalcite. Am Mineral 2002;87:623–9. https://doi.org/10.2138/am-2002-5-604.
[60] Vaiciukyniene D, Baltakys K, Kantautas A. Hydrosodalite ion exchange in saturated $Ca(OH)_2$ solution. Mater Sci-Poland 2009;27:417–26.
[61] Vogrin J, Santini T, Peng H, Vaughan J. The anion effect on sodium aluminosilicates formed under Bayer process digestion conditions. Hydrometall 2020;192:105236. https://doi.org/10.1016/j.hydromet.2019.105236.
[62] Dib E, Rey J, Vicente A, Kunjir S, Awala H, Komaty S, et al. Access to sodalite cages in ion-exchanged nanosized FAU zeolites probed by hyperpolarized 129Xe NMR and DFT calculations. Micropor Mesopor Mater 2022;338:111965. https://doi.org/10.1016/j.micromeso.2022.111965.
[63] Chukanov NV, Aksenov SM, Pekov IV. Infrared spectroscopy as a tool for the analysis of framework topology and extra-framework components in microporous cancrinite- and sodalite-related aluminosilicates. Spectrochim Acta A Mol Biomol Spectrosc 2023;287:121993. https://doi.org/10.1016/j.saa.2022.121993.
[64] Reyes CAR, Williams C, Alarcón OMC. Nucleation and growth process of sodalite and cancrinite from kaolinite-rich clay under low-temperature hydrothermal conditions. Mat Res 2013;16:424–38. https://doi.org/10.1590/S1516-14392013005000010.
[65] E. Kása, K. Baán, Zs. Kása, Z. Kónya, Á. Kukovecz, I. Pálinkó, P. Sipos, M. Szabados, The effect of mechanical and thermal treatments on the dissolution kinetics of kaolinite in alkaline sodium aluminate solution under conditions typical to Bayer desilication, App. Clay Sci. 229 (2022) 106671. Doi: 10.1016/j.clay.2022.106671.
[66] Palmer SJ, Frost RL, Nguyen T. Hydrotalcites and their role in coordination of anions in Bayer liquors: anion binding in layered double hydroxides. Coord Chem Rev 2009;253:250–67. https://doi.org/10.1016/j.ccr.2008.01.012.
[67] International Aluminium Institute, Alumina Production, 2025. https://international-aluminium.org/statistics/alumina-production (accessed 14 March 2026).
[68] Engelhardt G, Felsche J, Sieger P. The hydrosodalite system $Na_{6+x}[SiAlO_4]_6(OH)_x{\cdot}nH_2O$: formation, phase composition, and de- and rehydration studied by ^1H, ^{23}Na, and ^{29}Si MAS-NMR spectroscopy in tandem with thermal analysis, X-ray diffraction, and IR spectroscopy. J Am Chem Soc 1992;114: 1173–82. https://doi.org/10.1021/ja00030a008.
[69] Deng Y, Flury M, Harsh JB, Felmy AR, Qafoku O. Cancrinite and sodalite formation in the presence of cesium, potassium, magnesium, calcium and strontium in Hanford tank waste simulants. Appl Geochem 2006;21:2049–63. https://doi.org/10.1016/j.apgeochem.2006.06.019.
[70] Chukanov NV, Vigasina MF, Zubkova NV, Pekov IV, Schäfer C, Kasatkin AV, et al. Extra-framework content in sodalite-group minerals: complexity and new aspects of its study using infrared and Raman spectroscopy. Minerals 2020;10:363. https://doi.org/10.3390/min10040363.
[71] Gilani NS, Tilami SE, Azizi SN. One-step green synthesis of nano-sodalite zeolite and its performance for the adsorptive removal of crystal violet. J Chin Chem Soc 2021;68:2264–73. https://doi.org/10.1002/jccs.202100258.
[72] Catarino M, Martins S, Dias APS, Costa Pereira MF, Gomes J. Calcium diglyceroxide as a catalyst for biodiesel production. J Environ Chem Eng 2019;7: 103099. https://doi.org/10.1016/j.jece.2019.103099.
[73] Zahoransky T, Friis H, Marks MAW. Luminescence and tenebrescence of natural sodalites: a chemical and structural study. Phys Chem Minerals 2016;43:459–80. https://doi.org/10.1007/s00269-016-0810-0.
[74] Hettman K, Wenzel T, Marks M, Markl G. The sulfur speciation in S-bearing minerals: New constraints by a combination of electron microprobe analysis and

DFT calculations with special reference to sodalite-group minerals. Am Mineral 2012;97:1653–61. https://doi.org/10.2138/am.2012.4031.
[75] Mikuła A, Król M, Koleżyński A. The influence of the long-range order on the vibrational spectra of structures based on sodalite cage. Spectrochim Acta A Mol Biomol Spectrosc 2015;144:273–80. https://doi.org/10.1016/j.saa.2015.02.073.
[76] Moloy EC, Liu Q, Navrotsky A. Formation and hydration enthalpies of the hydrosodalite family of materials. Micropor Mesopor Mater 2006;88:283–92. https://doi.org/10.1016/j.micromeso.2005.09.020.
[77] Alvarez MG, Segarra AM, Contreras S, Sueiras JE, Medina F, Figueras F. Enhanced use of renewable resources: transesterification of glycerol catalysed by hydrotalcite-like compounds. Chem Eng J 2010;161:340–5. https://doi.org/10.1016/j.cej.2009.12.036.
[78] Wu Y, Song X, Cai F, Xiao G. Synthesis of glycerol carbonate from glycerol and diethyl carbonate over Ce-NiO catalyst: the role of multiphase Ni. J Alloy Comp 2017;720:360–8. https://doi.org/10.1016/j.jallcom.2017.05.292.
[79] Wu Y, Song X, Zhang J, Li S, Yang X, Wang H, et al. Synthesis of glycerol carbonate from glycerol and diethyl carbonate over CeO_2-CdO catalyst: the role of Ce^{4+} doped into CdO lattice. J Taiwan Inst Chem E 2018;87:131–9. https://doi.org/10.1016/j.jallcom.2017.05.292.
[80] Souza Jr RL, Rossi TM, Detoni C, Souza MMVM. Glycerol carbonate production from transesterification of glycerol with diethyl carbonate catalyzed by Ca/Al-mixed oxides derived from hydrocalumite. Biomass Conv Bioref 2023;13:661–73. https://doi.org/10.1007/s13399-020-01110-4.
[81] Andola SC, Pandey A, Kothari AC, Singh G, Singh A, Malik R. Green synthesis of glycerol carbonate from glycerol over prepared sodium aluminate catalysts by spray drying. Catal Lett 2025;155:242. https://doi.org/10.1007/s10562-025-05081-x.
[82] Rani GS, Jyotsna A, Devi BLAP. Carbon-SO_3Na catalysed synthesis of glycerol carbonate via transesterification of glycerol and dimethyl carbonate. ChemistrySelect 2022;7:e202202798. https://doi.org/10.1002/slct.202202798.
[83] Liu Z, Liu Z, Li B, Qiao F, Zhang Y, Wang X, et al. Catalytic performance of Li/Mg composites for the synthesis of glycerol carbonate from glycerol and dimethyl carbonate. ACS Omega 2022;7:5032–8. https://doi.org/10.1021/acsomega.1c05968.
[84] Yu J, Wang K, Shao S, Li W, Du S, Chen X, et al. Effect of ionic radius and valence state of alkali and alkaline earth metals on promoting the catalytic performance of La_2O_3 catalysts for glycerol carbonate production. Chem Eng J 2023;458:141486. https://doi.org/10.1016/j.cej.2023.141486.
[85] Wang D, Bai D, Xiong J, Chen Z, Zhao X, Wu H, et al. The atom-efficient production of glycerol carbonate via transesterification between dimethyl carbonate and glycerol over fluorinated Al_2O_3-ZrO_2 solid solution catalysts with suitable acidic-basic property. Appl Catal A-Gen 2023;665:119370. https://doi.org/10.1016/j.apcata.2023.119370.
[86] Argüello DS, Saavedra CC, Mendoza SM, Oliva MI, Rodríguez-Castellón E, Bálsamo NF, et al. Layered double hydroxides modified by transition metals for sustainable glycerol valorization to glycerol carbonate. Catal Today 2024;427:114415. https://doi.org/10.1016/j.cattod.2023.114415.
[87] Jitjamnong J, Khongprom P, Ratanawilai T, Ratanawilai S. Glycerol carbonate synthesis via transesterification of enriched glycerol and dimethyl carbonate using a Li-incorporated MCM-41 framework. RSC Adv 2024;14:5941–58. https://doi.org/10.1039/D4RA00290C.
[88] Dube ST, Qwabe LQ, Friedrich HB. Modified basicity of Mg-Fe mixed metal oxides catalysts for glycerol conversion to form glycerol carbonate via the transesterification route. Appl Catal O: Open 2025;206:207065. https://doi.org/10.1016/j.apcato.2025.207065.
[89] Malaika A, Rachela M, Kozłowski M. Transesterification of glycerol to glycerol carbonate over alkali carbonate-carbon hybrid catalysts. ChemCatChem 2025;17:e202500143. https://doi.org/10.1002/cctc.202500143.
[90] Lian J, Zhang L, Xia L, Wang L, Zhou X, Lin S, et al. Highly efficient synthesis of glycerol carbonate over CuO/ZnO/MnO_2 catalyst. Mater Today Chem 2025;43:102523. https://doi.org/10.1016/j.mtchem.2025.102523.
[91] Yu B-Y, Wu P-J, Tsai C-C, Lin S-T. Evaluating the direct CO_2 to diethyl carbonate (DEC) process: rigorous simulation, techno-economical and environmental evaluation. J CO2 Util 2020;41:101254. https://doi.org/10.1016/j.jcou.2020.101254.
[92] Pattanaik PP, Pradhan S, Bej A, Pradhan G. Solid waste derived heterogeneous catalysts for synthesis of sustainable glycerol carbonate from glycerol. Biomass Bioenergy 2025;193:107598. https://doi.org/10.1016/j.biombioe.2025.107598.
[93] Chalermthai B, Sriharuethai C, Olsen BD, Ngaosuwan K, Soottitantawat A, Assabumrungrat S, et al. Comparative study of conventional and process intensification by reactive distillation designs for glycerol carbonate production from glycerol and diethyl carbonate. Sci Rep 2025;15:1753. https://doi.org/10.1038/s41598-025-85974-4.